JAIST Repository
https://dspace.jaist.ac.jp/

Title	Material properties of pulsed-laser crystallized Si thin films grown on yttria-stabilized zirconia crystallization-induction layersby two-step irradiation method
Author(s)	Lien, Mai Thi Kieu; Horita, Susumu
Citation	Japanese Journal of Applied Physics, 55(3S1): 03CB02-1-03CB02-8
Issue Date	2016-02-19
Type	Journal Article
Text version	author
URL	http://hdl.handle.net/10119/14045
Rights	This is the author's version of the work. It is posted here by permission of The Japan Society of Applied Physics. Copyright (C) 2016 The Japan Society of Applied Physics. Mai Thi Kieu Lien and Susumu Horita, Japanese Journal of Applied Physics, 55(3S1), 2016, 03CB02-1-03CB02-8. http://dx.doi.org/10.7567/JJAP.55.03CB02
Description	

JAIST
JAPAN
ADVANCED INSTITUTE OF
SCIENCE AND TECHNOLOGY

Japan Advanced Institute of Science and Technology

Material Properties of Pulsed-Laser Crystallized Si Thin Films Grown on YSZ Crystallization-Induction Layers by Two-Step Irradiation Method

Mai Thi Kieu Lien and Susumu Horita

School of Materials Science, Japan Advanced Institute of Science and Technology, Nomi, Ishikawa 923 – 1292, Japan

E-mail: mtklien@ued.udn.vn; horita@jaist.ac.jp

Amorphous Si thin films on YSZ layers were crystallized widely in solid phase by the two-step method with pulsed laser, moving the sample stage. The crystalline quality, impurity diffusion, and electrical properties of the crystallized Si films were investigated. It was found that crystallinity of Si film was improved and its surface was quite smooth without incubation layer at the interface, indicating uniform crystallinity of the Si on the YSZ. The diffusion of Zr and Y into the crystallized Si film was as small as or smaller than the order of 10^{17} atoms/cm^3. We evaluated the electrical properties of carrier concentration and Hall mobility of Si thin films with/without YSZ layers by using the resistivity and AC Hall effect measurements. The temperature and doping concentration dependences were measured for both undoped and P-doped films. It was found that both the undoped and P-doped Si/YSZ/glass films showed higher mobilities and carrier concentrations (therefore higher conductivities), which means smaller amount of defects, than those of the Si/glass. This suggested that the Si film crystallized on the YSZ layer is more suitable for application of electronic devices, compared with the Si film on glass.

1. Introduction

In thin-film transistor (TFT) fabrication, although oxide[1-3] and organic materials[4,5] have been studied extensively for active channel material, the most prolonged and widely used materials are hydrogenated-amorphous silicon (a-Si:H)[6] and polycrystalline silicon (poly-Si)[7]. The a-Si:H TFT can be fabricated at a lower cost than poly-Si TFT. However, low carrier mobility (~ $1 cm^2 V^{-1} s^{-1}$), instability, and low reliability[8-10] are its drawbacks, which can be addressed by poly-Si TFT. As a fabrication method, generally, crystallization of deposited a-Si films has been widely used to obtain high quality films. It can be carried out by several techniques, such as solid phase crystallization (SPC),[11-15] metal-induced crystallization (MIC),[16-19] metal-induced lateral crystallization (MILC),[20-23] and pulsed laser annealing (PLA).[24-27] Among them, although PLA has become a leading technique to fabricate poly-Si films at low temperature, high surface roughness and non-uniform-sized grain in the melted poly-Si films limit the extent of applications. To overcome these limitations, we proposed using a crystallization-induction (CI) layer of yttria-stabilized zirconia [$(ZrO_2)_{1-x}(Y_2O_3)_x$:YSZ][28,29] combined with PLA for micro-crystallization with non-intentional melting.[30,31] It was found that, the grain size of poly-Si film on YSZ layer is more uniform than that on glass due to the CI effect of YSZ layer based on its crystal property, which are a small lattice mismatch and the same cubic crystal structure as Si. To further improve the crystallinity of Si films, we have proposed the two-step method in PLA.[32–34] Firstly, a-Si films are irradiated at a low initial energy P_i to generate nuclei, following by irradiation at a high growth energy P_g to accelerate the nuclei growth and film crystallization without random nucleation in the bulk. It was found that crystallinity of Si films is much improved by using the two-step method, compared with the one-step (or

conventional) method with a fixed energy.

In this paper, we first show the investigation results on crystalline quality of crystallized Si films on the glass substrates with/without the YSZ layers by the two-step method in PLA, comparing with the one-step method. Then, we show the temperature and doping concentration dependences of electrical properties of carrier concentration n and mobility μ_H, which were measured by alternative current (AC) Hall effect measurement using the Van der Pauw method. Generally, it is very difficult to measure low conductive thin films or low carrier concentrations by direct current (DC) Hall effect measurement because of small signal (S) to noise (N) or low S/N ratio. This time, by using the AC measurement, it was possible to estimate such low conductive films. From the results, we will discuss on the CI effect of YSZ layer on the electrical properties.

2. Experimental procedure

A 60 nm YSZ (111)-CI layer[31)] is deposited on a cleaned fused quartz glass substrate at a substrate temperature of 50 ^{o}C by reactive magnetron sputtering. The yttrium content ratio R = Y/Zr of the as-deposited YSZ layer is about 0.2. Then, a 60 nm a-Si film is deposited on a YSZ/quartz substrate by e-beam evaporation at 300 ^{o}C and 1×10^{-8} Torr. For comparison, an a-Si film is also deposited directly on a quartz substrate without a YSZ layer. For investigating electrical properties, undoped and doped samples are prepared. In the doping case, a SiO_2 capping layer with the thickness of 50~60 nm is deposited by atmospheric pressure chemical vapor deposition (APCVD) at 200 ^{o}C after cleaning the as-deposited a-Si film. Then, it is annealed in N_2 ambient at 350 ^{o}C for 30 min. Next, P ion implantation is

performed on the whole Si films, in which an acceleration voltage and ion dose are changed from 40 to 50 kV and from 4.44×10^{12} to 5.56×10^{14} cm^{-2}, respectively. In this case, the average doping concentration in the whole a-Si film is varied from 3.7×10^{17} to 4.9×10^{19} cm^{-3}. Subsequently, the capping layer is removed, following by crystallization of the a-Si films in solid phase by PLA together with activation of the implanted P dopants in N_2 ambient. For this annealing, we use the two-step method as shown in Fig. 1 schematically. The pulsed laser is Nd:YAG laser (λ = 532 nm) with a repetition frequency of 10 Hz, a pulsed duration of 6~7 ns, and a 4-mm-diameter. The total crystallized area is 10×20 mm^2 by moving the samples held on a stage with a pulse motor and fixing the laser optical line, where the moving speed v is 1 mm/s and the moving distance per one shot is 100 μm. In this experiment, the initial energy P_i and growth energy P_g are set 6.3 and 15 mJ/pulse, respectively, which correspond to the optimized energy densities in the static case without moving a sample for the Si/YSZ/glass structure.[34)] For comparison, some samples without doping are also prepared by a one-step method at a fixed high energy of P_g. After crystallization, a 135-nm-thick SiO_2 passivation layer is deposited by APCVD at 200 ^oC, followed by post-annealing in N_2 ambient at 350 ^oC for 30 min. A Hall effect measurement patterns are formed and Al metal electrodes are deposited by vacuum evaporation. Finally, sintering process is carried out at 350 ^oC in N_2 for 30 min. The Hall patterns for the undoping cases are formed after the same processes as those of the doping cases except deposition of a SiO_2 capping layer and P ion implantation.

The crystallization degrees of the Si films without doping are locally estimated by He-Cd Raman spectroscopy with a wavelength of 442 nm. The absorption depths for a-Si and poly-Si are 20–30 nm and more than 200 nm, respectively. Therefore, it is used to evaluate the

crystalline quality locally at the surface and interface of the Si films. The cross-section of the crystallized Si films on the YSZ/glass substrate without doping was observed by transmission electron microscopy (TEM). The surface crystallinity of Si films with/without the YSZ layer is observed by *in situ* reflection high-energy electron diffraction (RHEED) after crystallization. Depth profiles of Zr and Y in the crystallized Si film on the YSZ layer are measured by secondary ion mass spectroscopy (SIMS) in order to investigate the diffusion of impurities in the Si films. Carrier concentration n and Hall mobility μ_H of the crystallized Si films are measured by the resistivity and AC Hall effect measurements with a magnetic field of 0.4 T by Model 8403, TOYO Corporation, using the Van der Pauw method. The final pattern is formed as shown in Fig. 2 from the top-view, where the regions 1, 2, 3, and 4 are for contacting, and the area 5 is a main region for measurement. As the diameter of the region 5 is roughly 7 mm, the measurement results show average results of n and μ_H over in-grains and grain boundaries. So, probably the measured μ_Hs are much lower than in-grain ones as the previous reports.[35,36] Since the voltage-current relationships between two terminals are always linear, the contacts are well ohmic. Hall voltages are found to be proportional to the applied magnetic field and excitation current. For each measurement, the polarity of excitation current is reversed and the Hall voltages in both directions were averaged over three readings for calculating the carrier concentration and mobility. The measurement temperature is varied by two directions of the change in temperature, i.e., from room temperature (RT) to 300 ^{o}C and from 300 ^{o}C to RT in vacuum atmosphere within the variation of ± 0.5 ^{o}C. Both the results for the two directions are almost the same. In this paper, the results are shown for the direction from 300 ^{o}C to RT for

simplification of data expression. From the temperature dependence results, activation energies of n and μ_H are estimated.

3. Results and discussion

3.1 Film structure and impurity

Figure 3 shows the comparison of the He-Cd Raman spectra of crystallized Si films between the one-step (with a fixed beam energy) and two-step methods. The (a) and (b) are obtained from the front side of the Si film surface and back side of the glass substrate, respectively, irradiated by the He-Cd laser beams. It can be seen that Raman intensities from the front side and back side measurements for the two-step method are much higher than those of the one-step method. Also, higher Raman intensities with smaller shoulders of a-Si phase (denoted by the dashed circles) can be seen from the both front and back side measurements, compared with those of the one-step method. This result indicates that crystallinity of the Si films is improved by the two-step method in the case of moving during irradiation as well as non-sample moving or static case, which has been mentioned in the previous paper. [34] Moreover, in the two-step method, the Raman intensity obtained from the back side measurement is about twice higher with a smaller shoulder of a-Si phase, showing the smaller FWHM of c-Si peak and higher crystalline fraction than those from the front side. It is considered that the interface crystallization in the two-step method proceeds better than the surface crystallization. On the other hand, the Raman intensities of both side measurements for the one-step method are almost same. This indicates that the surface and interface crystallizations by the one-step method occur simultaneously as well as in film bulk without preference.

Since thickness of the Si film is thin (~ 60 nm) and the grain size is small and roughly less than 200 nm, it was found that estimation of its crystallinity by X-ray diffraction technique was difficult. Therefore, we used RHEED technique to observe the surface crystalline structure of the Si films. Figures 4(a), (b), (c), and (d) show RHEED patterns of the bare YSZ layer on the glass substrate, a-Si film on the YSZ/glass, crystallized Si film on the YSZ/glass, and crystallized Si film on the glass at room temperature, respectively. The Si films were crystallized by the two-step method under condition of Fig. 1. All of these patterns were observed at room temperature. In Fig. 4(a), a clear spotty pattern is observed, which indicates a highly oriented YSZ film surface. It is found that the YSZ layer is uniaxially (111)-oriented as shown in the previous report, which is in good agreement with the XRD pattern.[31)] The spotty patterns disappear after deposition of the a-Si film as shown in Fig. 4(b), which suggests that the deposited Si film is in amorphous phase completely. On the other hand, in Figs. 4(c) and 4(d), after crystallization of the a-Si films, the spotty patterns reappear, which confirms the crystallization of a-Si films. Moreover, the spotty patterns in Fig. 4(c) are more clear than in Fig. 4(d) and similar to those of the bare YSZ layer in Fig. 4(a). From this result, it can be inferred that the (111)-preferential orientation of the YSZ is transferred into the crystallized Si film, thanks to the crystallization-induction effect of the YSZ.

Figures 5(a) and (b) show the cross-sectional low-resolution and high-resolution (HR-) TEM images, respectively, of the Si film on the YSZ/glass crystallized by the two-step method under the condition of Fig. 1. The HR-TEM image in Fig. 5(b) shows a close-up image of one area around the interface. This also shows the electron-diffraction (ED) patterns simulated by using the fast Fourier transform (FFT) based on the local lattice

images enclosed by white (labeled as points 1 and 3) and black (labeled as points 2 and 4) square frames in the YSZ layer and the crystallized Si film, respectively. It can be seen from Fig. 5(a) that the crystallized Si film has a smooth surface, which is probably due to non-intentionally melting crystallization of the Si film, compared with the direct deposited Si film at 430 ^{o}C[29] and melting crystallized Si film by excimer pulsed laser.[37] Further, an incubation layer near the YSZ layer interface is hardly observed, suggesting that crystallization of the Si film grows directly from the YSZ layer without an amorphous transition region. This is confirmed by the HR-image in Fig. 5(b). All spots in the ED patterns of the YSZ layer (points 1 and 3) and the Si film (points 2 and 4) correspond to {111} planes, except for the two spots of YSZ {200} indicated by white arrows. From these patterns, the crystallographic orientation normal to the interface can be identified as <111>, which is the preferential orientation of the YSZ layer. From this result, it can be considered as follows: Nucleation at the YSZ interface is stimulated by the CI effect of the YSZ layer, and then crystallization of the amorphous region around the nuclei occurs and progresses up to the surface smoothly. The slight roughness at the interface is just localized and due to the surface roughness of the YSZ layer.

The impurities in the Si film were measured by SIMS. Figure 6 shows the concentration depth profiles of Zr and Y in the 50-nm-thick Si film crystallized on the YSZ/glass substrate by the two-step method. Since the quantitative concentrations were estimated by using a standard sample of an ion-implanted Si, only the concentrations in the Si film are valid. The concentrations near the interface and in the YSZ layer are incorrect because of the so-called matrix and charge-up effects due to the insulator of YSZ.[38] It can be seen that Zr atoms diffuse into the crystallized Si film slightly and that the Zr concentration at the Si/YSZ

interface is about 3×10^{17} atoms/cm^3. The Zr concentration at the Si/YSZ interface in this work is about one order smaller than that in the direct deposited Si film at 430 ^{o}C (about 5×10^{18} atoms/cm^3).[29] This shows the effectiveness of the two-step method using a pulsed laser in suppression of Zr diffusion into the Si film. The Y concentration at the Si/YSZ interface is about 9×10^{16} atoms/cm^3, which is in rough agreement with the as-deposited chemical composition ratio R ≈ 0.2. It has been reported that, in the application of a gate insulator, Zr atoms from the ZrO_2 film hardly diffuse into Si even at 700 ^{o}C for 5 min annealing.[39] The diffusion of Y from Y_2O_3 gate oxide into the Si film also does not occur at annealing temperature ≤ 800 ^{o}C for 2 min.[40] In our case, a certain amounts of chemically unstable Zr and Y due to HF dipping might remain on the YSZ surface before the Si film deposition. Although it is supposed that the subsequent crystallization by the pulsed laser is performed at temperature less than the melting temperature of a-Si – 1420 K or 1147 ^{o}C,[41] it maybe induce the diffusion of Zr and Y into the Si film even for a very short irradiation time. From this result, we can consider that the diffusion of Zr and Y into the crystallized Si film from the YSZ layer is small, but they should be further suppressed for device application.

3.2 Electrical properties

Figures 7(a) and (b) show the temperature T dependences of carrier concentration n and Hall mobility μ_H for the undoped and P-doped Si films on the **glasses** with different average doping concentrations. The Si films were crystallized by the two-step method under the condition of Fig. 1. The labels of E_{ni} and $E_{\mu i}$ are activation energies for n and μ_H, respectively, which are calculated by least squares method, are also shown in Fig. 7. The

subscript “i” indicates an integer of 1 to 5. The solid black line in Fig. 7(a) shows the intrinsic concentration of Si for a reference. It is found that all of the Si films are n-type or the carriers are electrons. In Fig. 7(a), at the low doping concentration of 3.7×10^{17}cm^{-3}, the carrier concentrations are almost the same as those of the undoped film at any measurement temperature except the room temperature (RT). The value at RT is probably due to a process contamination by accident. Increasing the doping concentration, the carrier concentration increases with it too, and the temperature dependence disappears or the activation energy is almost zero. In Fig. 7(b), the Hall mobilities for the low doped film of 3.7×10^{17}cm^{-3} are slightly higher than those of undoped film at any measurement temperature. However, at a higher doping concentration of 4.9×10^{18}cm^{-3}, mobilities abruptly decrease and the activation energy E_{μ} becomes higher. Further doping, Hall mobility increases again with the lower E_{μ}.

Figures 8(a) and (b) show the measurement temperature T dependences of carrier concentration n and Hall mobility μ_{H} for the crystallized undoped and P-doped Si films on the **YSZs/glasses** under the same fabrication and measurement conditions of Fig. 7. We can see from Fig. 8(a) that, on the whole, the carrier concentrations increase with the measurement temperature and doping concentration. For the undoped case, the activation energy is changed from E_{n1} = 0.23 to E_{n2} = 0.46 eV around 100 ºC. Increasing the doping concentration to 3.7×10^{17}cm^{-3}, the activation energy E_{n3} is lowered to 0.22 eV from E_{n1}. Further increasing the doping concentration to 4.9×10^{18} cm^{-3} and higher, the carrier concentrations become higher too, and the temperature dependence disappears as shown in Fig. 8(a). The Hall mobility tendency in Fig. 8(b) is almost the same with the carrier concentration, i.e., μ_{H} increases with T and doping concentration, except in the high temperature region of 4.9×10^{18} cm^{-3}. The detailed explanation on the whole will be

summarized and discussed later, comparing with the results of Fig. 7(a) and (b) for the Si/glass case. In Fig. 8(b) for the undoped film, the activation energy of μ_H corresponding to mobility barrier height rapidly increases from $E_{\mu 1}$ = 0.02 eV to $E_{\mu 2}$ = 0.09 eV with increasing temperature in spite of the increase of μ_H. This seems contrary to a general concept, in which a Hall mobility decreases when a barrier height becomes higher. This might be explained by tunneling effect. In fact, the possibility of the tunneling effect on carrier transportation has been reported previously in the poly-Si film.[35,42)] Taking the tunneling effect into account, the barrier height should be reduced effectively. At the high temperature region (100 $^oC \leq T \leq$ 300 ^oC), the barrier width may be more extended than in the lower temperature due to a larger thermal energy. Because extension of the barrier width suppresses the tunneling effect of electron transportation, the effective activation energy of $E_{\mu 2}$ increased to be 0.09 eV and higher than $E_{\mu 1}$. Further, in Fig. 8(b), it is questionable that the mobility for the 4.9×10^{19} cm^{-3} increases with the temperature in spite of the lower E_μ = 0.01 eV than the thermal energy of 0.026 eV at RT. For simplification, the Hall mobility is expressed generally as $\mu_H = \mu_{Ho} \exp(-E_\mu/kT)$ with respect to T, where μ_{Ho} is a constant pre-factor and k is the Boltzmann constant. But, strictly speaking, according to the Seto's report,[35)] μ_H is proportional to $T^{(-1/2)} \exp(-E_\mu/kT)$, not only an exponential factor. Also, the paper mentioned that if $E_\mu > kT$, a relation between log (μ_H) versus (vs) $1/T$ should yield a straight line with a negative slope of E_μ. So, the lower E_μs including E_μ = 0.01 eV are not adequate estimation values as activation energies and E_μs were reestimated by plotting log ($\mu_H \cdot T^{1/2}$) vs $1/T$. As a result, we obtain the corrected values, for example, $E_{\mu 5}'$ = 0.04 eV from the previous value of 0.03 eV for the **Si/glass** in Fig. 7(b), and $E_{\mu 5}'$ = 0.03 eV from the previous value of 0.01 eV for the **Si/YSZ/glass** in Fig. 8(b). Therefore, the lower $E_{\mu 5}$s

estimated in Figs. 7(b) and 8(b) are not corrected and the actual ones are higher than them. Since this is not essential issue for this paper, it is not further discussed.

In order to discuss the behaviors of electrical properties more in detail, Figs. 9(a) and (b) show the summaries of the doping concentration dependences of carrier concentration and its activation energy, and the doping concentration dependences of Hall mobility and its activation energy, respectively, for the Si films on the **glasses** at RT. In Fig. 9(a), the solid black line shows the carrier concentration–equal to the doping concentration or 100 % activation line. It can be seen from Fig. 9(a) that, for the undoped and low doped films, the carrier concentrations n is much lower than the doping concentration and the activation energies E_ns are almost the same near the intrinsic Fermi level E_i. This indicates that the E_ns should be trap levels. Increasing the doping concentration up to the middle of 10^{18} cm^{-3}, the carrier concentration increases rapidly whereas its activation energy decreases abruptly to around the ionization energy of P dopants (~0.045 eV).[43] Further increasing the doping concentration, the carrier concentration further increases and the activation energy decreases. These results can be explained by segregation of doped P atoms and their passivation effect on crystalline defects of grain boundary and bulk film as well-known.[44]

From Fig. 9(b), it is found that the Hall mobility μ_H and its activation energy E_μs for the undoped and low doped around middle of 10^{17} cm^{-3} films are almost the same. This is because the free electrons hardly move due to the large amount of crystalline defects as mentioned above. Increasing the doping concentration to around the middle of 10^{18} cm^{-3}, the μ_H decreases to a minimum whereas the E_μ or barrier height reaches a maximum. This is because the thermally activated electrons are more trapped at the GBs, which extends the depletion regions around the GBs. The doping concentration around the middle of 10^{18} cm^{-3}

is considered as the critical value at which the depletion regions reach maxima or the grains are fully depleted. Further doping, the barrier height or E_μ is reduced due to the reduction of the depletion region. Free electrons can move easier and smoother. As a result, the μ_H increases again.

Figures 10(a) and (b) show the summaries of the doping concentration dependences of carrier concentration and its activation energy, and the doping concentration dependences of Hall mobility and its activation energy, respectively, for the undoped and P-doped Si films on the **YSZs/glasses** at RT. The solid black line also indicates the same in Fig. 9(a). Comparing Fig. 10(a) with Fig. 9(a), the carrier concentrations of the undoped and middle 10^{17} cm^{-3} doped Si films on the **YSZs/glasses** are higher than those of the Si films on the **glasses**. The activation energies E_ns of the formers are about half of those for the latters. These results suggest that the amount of crystalline defects in the Si films on the **YSZs/glasses** is much less than in the Si films on the **glasses**, or that the trap density is lower than that of the **Si/glass** case. At the higher doping concentration, behaviors of *n* and E_n of the Si/YSZ/glass case are similar to those of the Si/glass case in Fig. 9(a), but a little larger. Actually, the activation ratio of the Si/YSZ/glass is near 100 %, but that of the Si/glass is ~90 % at the doping concentration of 4.9×10^{19} cm^{-3}.

The Hall mobility of the Si films on the **YSZs/glasses** in Fig. 10(b) increases without a minimum. The maximum of activation energy E_μ shifts toward the lower doping concentration, compared with that of the Si films on the **glasses** in Fig. 9(b). This result is also considered due to the smaller amount of crystalline defects in the **Si/YSZ/glass** case, compared with the **Si/glass** case, which leads to the smaller E_μ or lower barrier height. As a result, free electrons can move more easily, leading to the higher Hall mobility.

A trap density N_t (cm^{-2}) at a grain boundary in a crystallized Si films is estimated by:[35,45)]

$$N_t = N^* \times L, \quad (1)$$

where N^* and L are the critical doping concentration (cm^{-3}) and average grain size of the crystallized Si film (cm), respectively. From the SEM image of our previous paper,[34)] the estimated average grain sizes for the **Si/glass** and **Si/YSZ/glass** are roughly ~50 nm and ~100 nm, respectively. Also, from Figs. 9(b) and 10(b), the N^* of the **Si/YSZ/glass** is estimated ~4×10^{17} cm^{-3}, which is about one order smaller than that of the **Si/glass** (~5×10^{18} cm^{-3}). Then, from eq. (1), it is found that the estimated trap densities for the **Si/YSZ/glass** is ~4×10^{12} (cm^{-2}) and about one order smaller than ~2.5×10^{13} (cm^{-2}) for the **Si/glass**.

4. Conclusions

The wide crystallization of Si films on YSZ crystallization-induction (CI) layers was achieved successfully under the crystallization condition by the two-step irradiation method with the pulsed laser, moving the sample during irradiation. The crystalline quality, impurity diffusion, and electrical properties of carrier concentration and Hall mobility of the crystallized Si films were investigated. The He-Cd Raman spectroscopy results revealed that the crystallinity of the Si films is improved by the two-step method. Furthermore, it was found from the RHEED measurement that the (111)-preferential orientation of the YSZ was transferred into the crystallized Si film, thanks to the CI effect of the YSZ. The TEM observation showed the smooth surface of crystallized Si film and no incubation layer at the interface. The SIMS results showed that the diffusion of Zr and Y from the YSZ layer into the crystallized Si film is as small as or smaller than the order of 10^{17} atoms/cm^3. The

resistivity and AC Hall effect measurements results for both the undoped and P-doped Si films revealed that higher mobility and carrier concentration (therefore higher conductivities) are obtained for the Si/YSZ/glass structure, compared with those of the Si/glass. Therefore, we can conclude that Si films crystallized on the YSZ layers are more suitable for application of electronic devices. From these results, we can expect a high performance of TFTs made from an Si film crystallized on the YSZ layer by the two-step method.

Acknowledgment

This work was partially supported by Marubun Research Promotion Foundation.

References

1) P. F. Carcia, R. S. McLean, M. H. Reilly, and G. Nunes, Jr., Appl. Phys. Lett. **82**, 1117 (2003).

2) K. Nomura, H. Ohta, K. Ueda, T. Kamiya, M. Hirano, and H. Hosono, Science **300**, 1269 (2003).

3) K. Nomura, H. Ohta, A. Takagi, T. Kamiya, M. Hirano, and H. Hosono, Nature **432**, 488 (2004).

4) C. D. Dimitrakopoulos and P. R. L. Malenfant, Adv. Mater. **14**, 99 (2002).

5) H. Y. Choi, S. H. Kim, and J. Jang, Adv. Mater. **16**, 732 (2004).

6) P. G. LeComber, W. E. Spear, and A. Ghaith, Electron. Lett. **15**, 179 (1979).

7) T. Sameshima, S. Usui, and M. Sekiya, IEEE Electron Device Lett. **7**, 276 (1986).

8) M. J. Powell, IEEE Trans. Electron Devices **36**, 2753 (1989).

9) M. J. Powell, Appl. Phys. Lett. **43**, 597 (1983).

10) F. R. Libsch and J. Kanicki, Appl. Phys. Lett. **62**, 1286 (1993).

11) C. Ipri and G. Kaganowicz, IEEE Trans. Electron Devices **35**, 708 (1988).

12) G. Liu and S. J. Fonash, Appl. Phys. Lett. **55**, 660 (1989).

13) R. Kakkad, J. Smith, W. S. Lau, S. J. Fonash, and R. Kerns, J. Appl. Phys. **65**, 2069 (1989).

14) L. Haji, P. Joubert, J. Stoemenos, and N. A. Economou, J. Appl. Phys. **75**, 3944 (1994).

15) J. N. Lee, Y. W. Choi, B. J. Lee, and B. T. Ahn, J. Appl. Phys. **82**, 2918 (1997).

16) S. F. Gong, H. T. G. Hentzell, A. E. Robertsson, L. Hultman, S. E. Hörnström, and G. Radnoczi, J. Appl. Phys. **62**, 3726 (1987).

17) G. Radnoczi, A. Robertsson, H. T. G. Hentzell, S. F. Gong, and M. A. Hasan, J. Appl. Phys. **69**, 6394 (1991).

18) S. Y. Yoon, K. H. Kim, C. O. Kim, J. Y. Oh, and J. Jang, J. Appl. Phys. **82**, 5865 (1997).

19) Z. Jin, G. A. Bhat, M. Yeung, H. S. Kwok, and M. Wong, J. Appl. Phys. **84**, 194 (1998).

20) S.-W. Lee, Y.-C. Jeon, and S.-K. Joo, Appl. Phys. Lett. **66**, 1671 (1995).

21) S.-I. Jun, Y.-H. Yang, J.-B. Lee, and D.-K. Choi, Appl. Phys. Lett. **75**, 2235 (1999).

22) M. Wong, Z. Jin, G. A. Bhat, P. C. Wong, and H. S. Kwok, IEEE Trans. Electron Devices **47**, 1061 (2000).

23) C.-Y. Hou and Y. S. Wu, Jpn. J. Appl. Phys. **44**, 7327 (2005).

24) J. C. C. Fan and H. J. Zeiger, J. Appl. Phys. **27**, 224 (1975).

25) T. Sameshima, M. Hara, and S. Usui, Jpn. J. Appl. Phys. **28**, L2131 (1989).

26) S. Higashi, N. Ando, K. Kamisako, and T. Sameshima, Jpn. J. Appl. Phys. **40**, 731 (2001).

27) S.-G. Ryu, I. Gruber, C. P. Grigoropoulos, D. Poulikakos, and S.-J. Moon, Thin Solid Films **520**, 6724 (2012).1) J. C. C. Fan and H. J. Zeiger, J. Appl. Phys. **27**, 224 (1975).

28) S. Horita and H. Sukreen, Appl. Phys. Express **2**, 041201(2009).

29) S. Horita and S. Hana, Jpn. J. Appl. Phys. **49**, 105801 (2010).

30) M. T. K. Lien, K. Mochizuki, and S. Horita, Proc. AM-FPD'13, 2013, p. 175.

31) M. T. K. Lien and S. Horita, Jpn. J. Appl. Phys. **53**, 03CB01 (2014).

32) M. T. K. Lien and S. Horita, Proc. of AM-FPD'14, 2014, p. 185.

33) M. T. K. Lien and S. Horita, Proc. IDW'13, 2013, p. 655.

34) M. T. K. Lien and S. Horita, Jpn. J. Appl. Phys. **54**, 03CA01 (2015).

35) J. Y. W. Seto, J. Appl. Phys. **46**, 5247 (1975).

36) S. Hasegawa, T. Kasajima, T. Shimizu, J. Appl. Phys. **50**, 7256 (1979).

37) A. Hara, K. Kitahara, K. Nakajima, and M. Okabe, Jpn. J. Appl. Phys. **38**, 6624 (1999).

38) R. G. Wilson, F. A. Stevie, and C. W. Magee, in *Secondary Ion Mass Spectroscopy* (Wiley, New York, 1989), Chap. 2.3.

39) W.-J. Qi, R. Nieh, B. H. Lee, L. Kang, Y. Jeon, K. Onishi, T. Ngai, S. Banerjee, and J. C. Lee, IEDM Tech. Dig., 1999, p. 145.

40) B. W. Busch, J. Kwo, M. Hong, J. P. Mannaerts, B. J. Sapjeta, W. H. Schulte, E. Garfunkel, and T. Gustafsson, Appl. Phys. Lett. **79**, 2447 (2001).

41) E. P. Donovan, F. Spaepen, D. Turnbull, J. M. Poate, and D. C. Jacobson, Appl. Phys. Lett. **42**, 698 (1983).

42) M. M. Mandurah, K. C. Saraswat, and T. I. Kamins, IEEE Trans. Electron Devices **ED-28**, 1163 (1981).

43) S. M. Sze and Kwok K. Ng. , in *Physics of Semiconductor Devices* (3rd edition), (John Willey & Sons, Inc., 2007), p. 22.

44) T. Kamins, in *Polycrystalline Silicon for Integrated Circuits and Displays* (2nd edition), (Klumer Academic Publishers, 1998), Sec. 3.6.

45) G. Baccarani, B. Ricco, and G. Spadini, J. Appl. Phys. **49**, 5565 (1978).

Figure captions

Fig. 1. (Color online) Schematic illustration for expansion of the crystallization area by moving the sample stage during irradiation with moving speed of 1 mm/s. The crystallization is performed by the two-step method in PLA.

Fig. 2. (Color online) Top-view illustration of the final Hall effect measurement pattern, which is a form of Van der Pauw pattern.

Fig. 3. (Color online) He-Cd Raman spectra of the **Si/YSZ/glass** for the one-step and two-step methods from (a) the front side or surface of crystallized Si film and (b) the back side or glass substrate measurements as shown in the insets.

Fig. 4. (Color online) RHEED patterns of the bare (a) YSZ layer on the glass substrate, (b) 60-nm-thick a-Si film on the YSZ/glass, (c) 60-nm-thick crystallized Si film on the YSZ/glass, and (d) 60-nm-thick crystallized Si film on the glass at room temperature.

Fig. 5. (Color online) Cross-sectional TEM images of the Si film on the YSZ/glass crystallized by the two-step method, where (a) is in low resolution and (b) is in high resolution (HR). The HR-TEM image (b) shows a close-up image around the interface in (a). The electron-diffraction patterns simulated based on the local lattice images enclosed by the white (points 1 and 3) and black (points 2 and 4) square frames for the YSZ layer and the crystallized Si film, respectively, are also shown.

Fig. 6. (Color online) Concentration depth profiles of Zr and Y in the crystallized Si/YSZ/glass by the two-step method. They were measured by SIMS. As a reference, the Si secondary ion intensity is shown.

Fig. 7. (Color online) Reciprocal measurement temperature dependences of (a) carrier concentration n and (b) Hall mobility μ_H for the undoped and P-doped Si films crystallized by the two-step method on the **glasses**.

Fig. 8. (Color online) Reciprocal measurement temperature dependences of (a) carrier concentration n and (b) Hall mobility μ_H for the undoped and P-doped Si films on the **YSZs/glasses** under the same fabrication and measurement conditions with Fig. 7.

Fig. 9. (Color online) (a) and (b) are the summaries of the doping concentration dependences of carrier concentration and its activation energy, and the doping concentration dependences of Hall mobility and its activation energy, respectively, for the undoped and P-doped Si films on the **glasses** at RT.

Fig. 10. (Color online) (a) and (b) are the summaries of the doping concentration dependences of carrier concentration and its activation energy, and the doping concentration dependences of Hall mobility and its activation energy, respectively, for the undoped and P-doped Si films on the **YSZs/glasses** at RT.

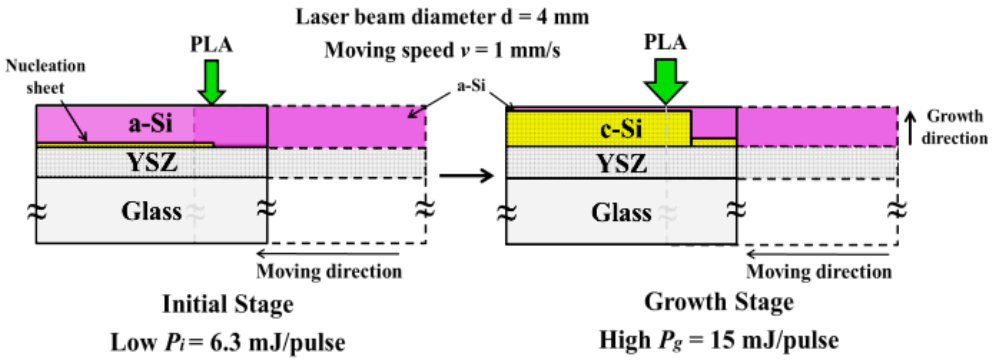

Fig. 1. Mai Thi Kieu Lien and Susumu Horita

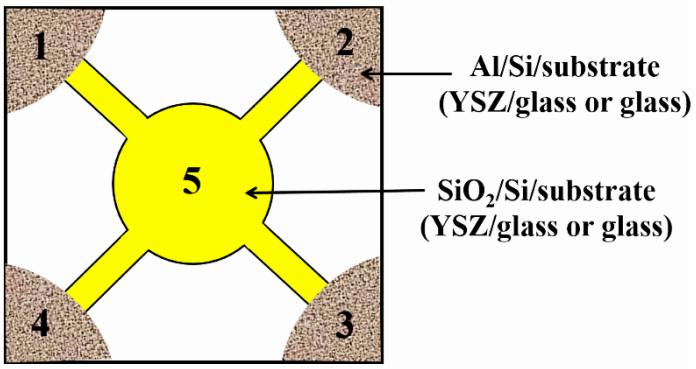

Fig. 2. Mai Thi Kieu Lien and Susumu Horita

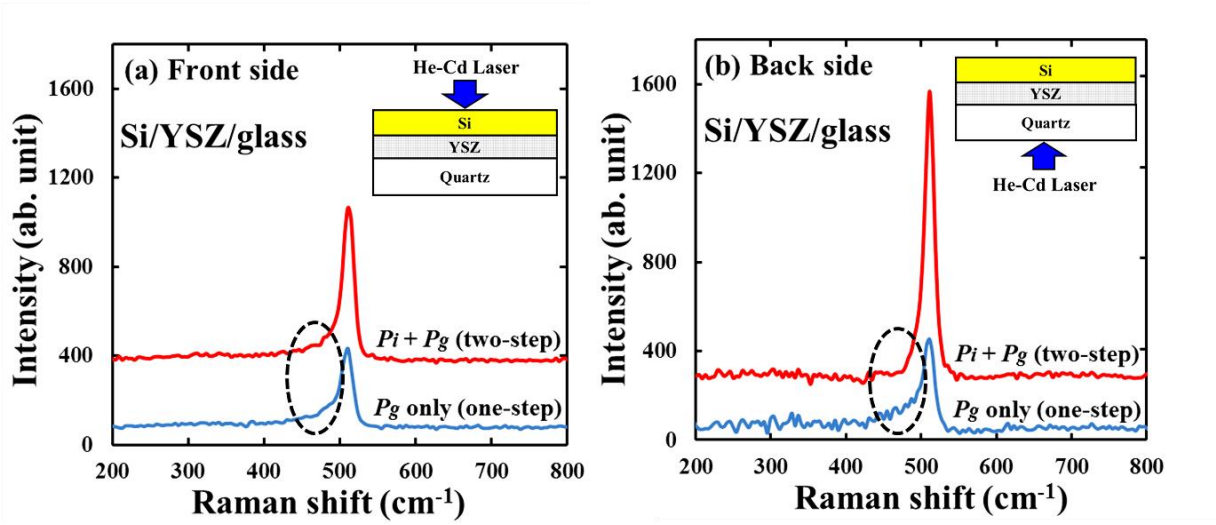

(a) **(b)**

Fig. 3. Mai Thi Kieu Lien and Susumu Horita

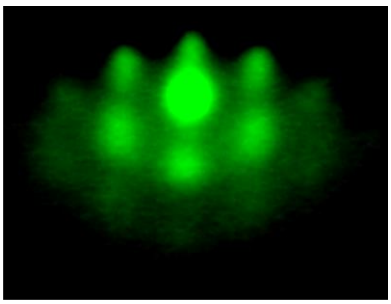

(a) bare YSZ layer

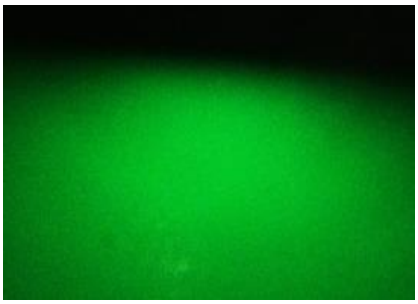

(b) a-Si/YSZ/glass

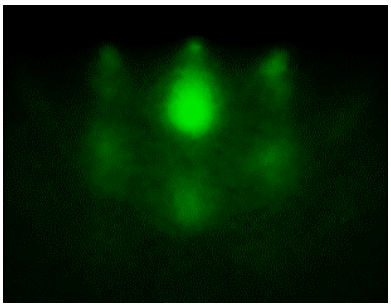

(c) crystallized Si/YSZ/glass

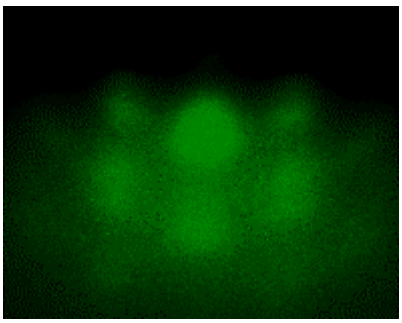

(d) crystallized Si/glass

Fig. 4. Mai Thi Kieu Lien and Susumu Horita

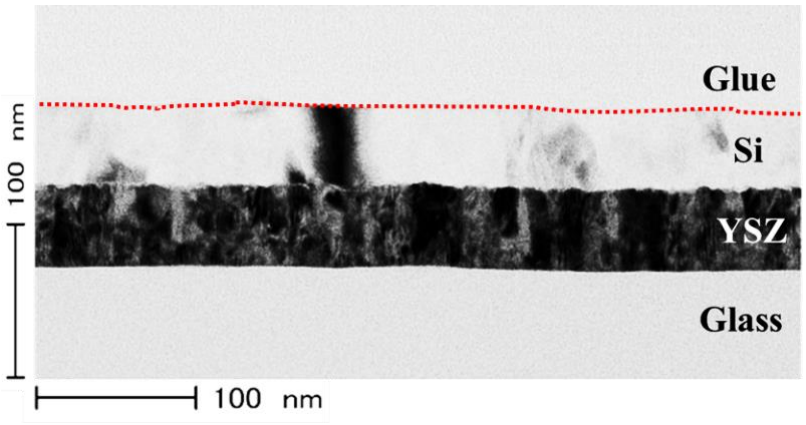

(a)

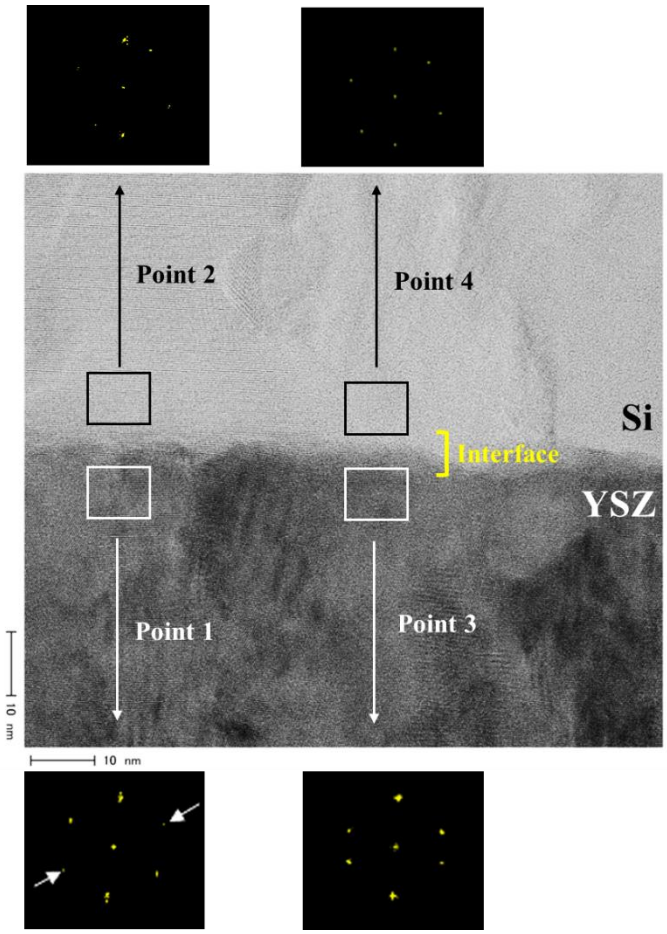

(b)

Fig. 5. Mai Thi Kieu Lien and Susumu Horita

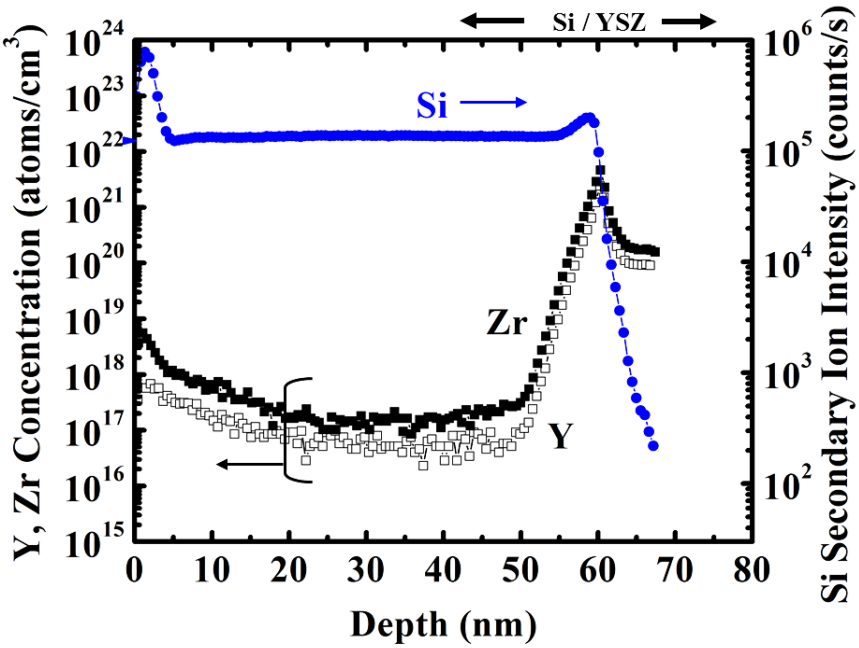

Fig. 6. Mai Thi Kieu Lien and Susumu Horita

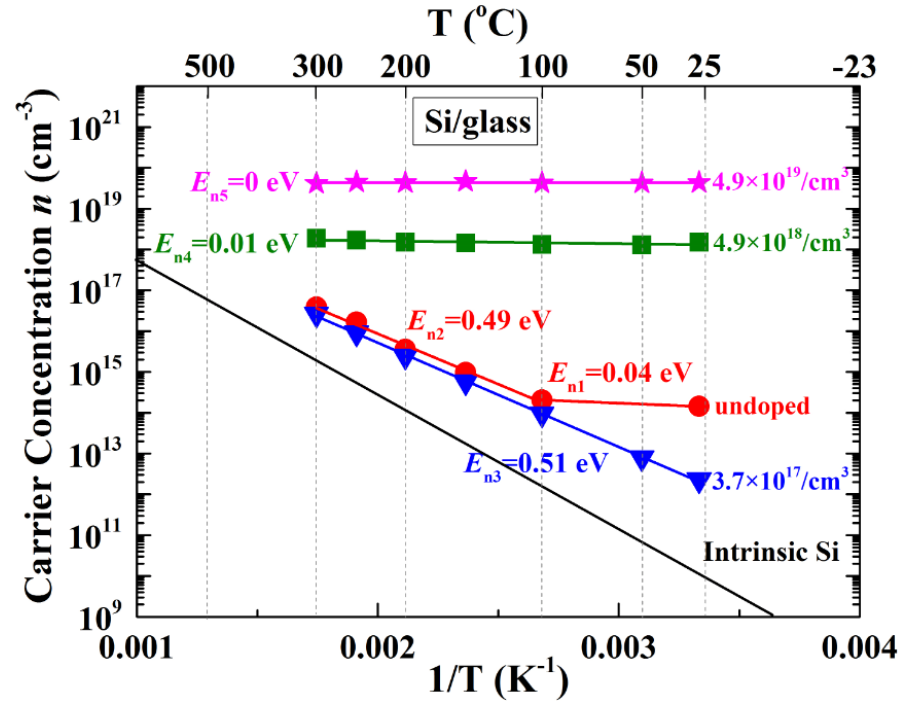

(a)

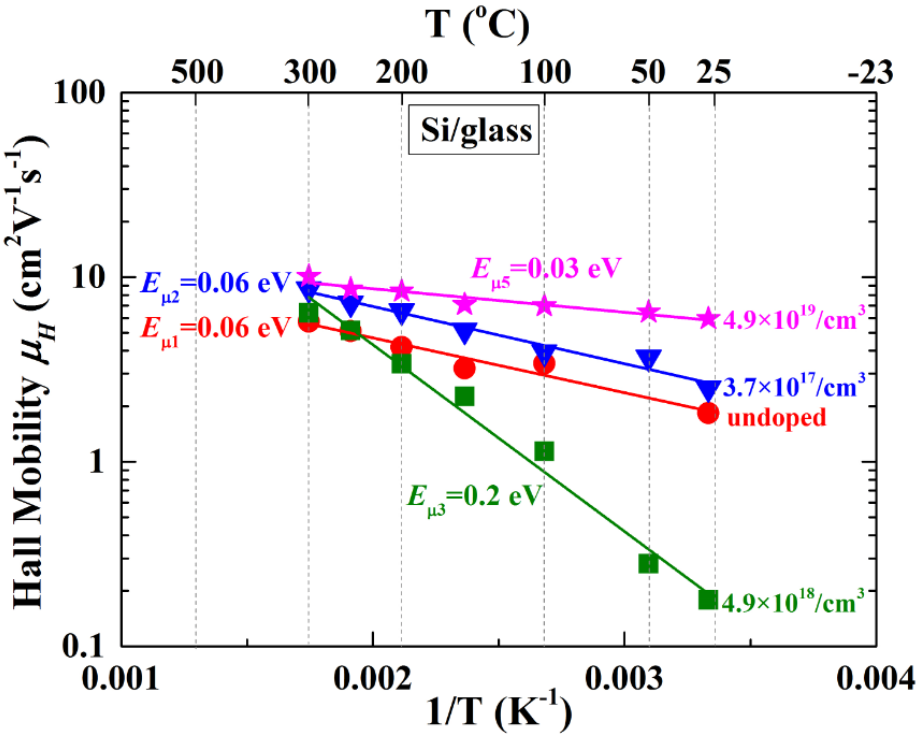

(b)

Fig. 7. Mai Thi Kieu Lien and Susumu Horita

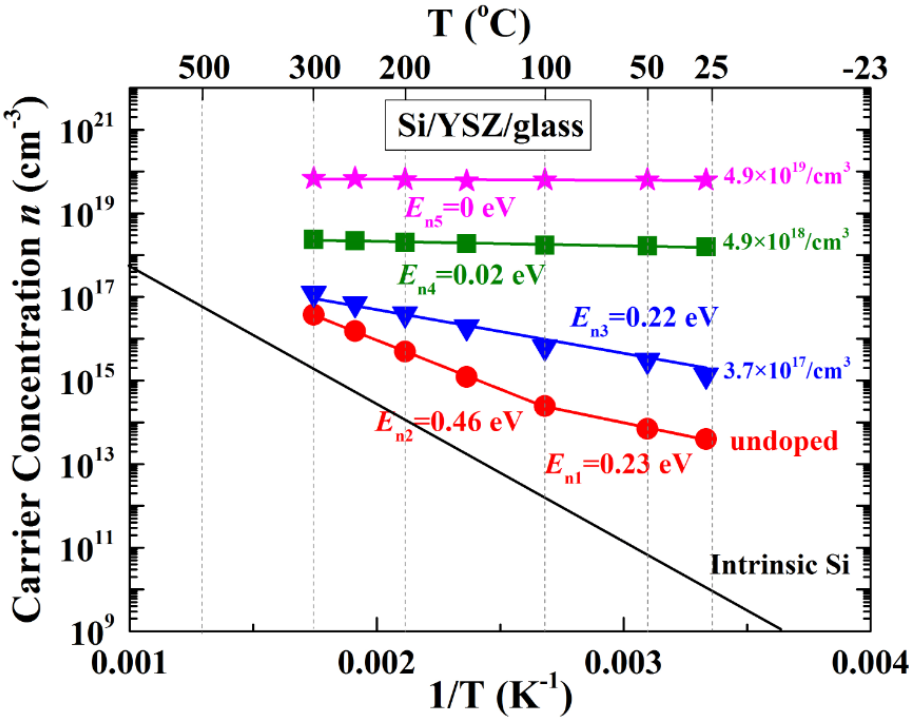

(a)

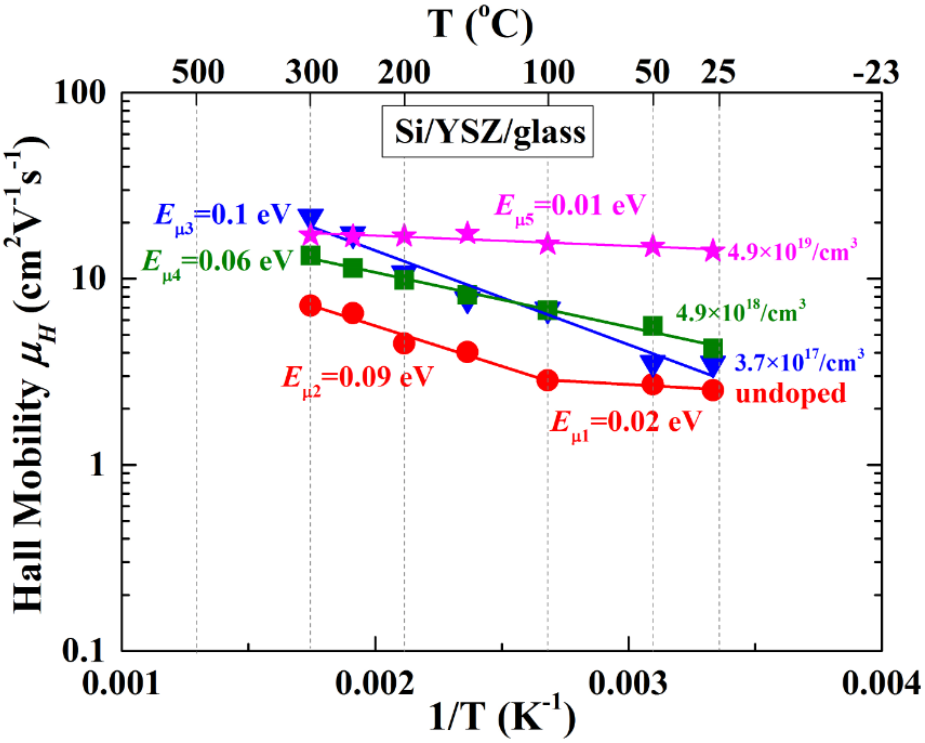

(b)

Fig. 8. Mai Thi Kieu Lien and Susumu Horita

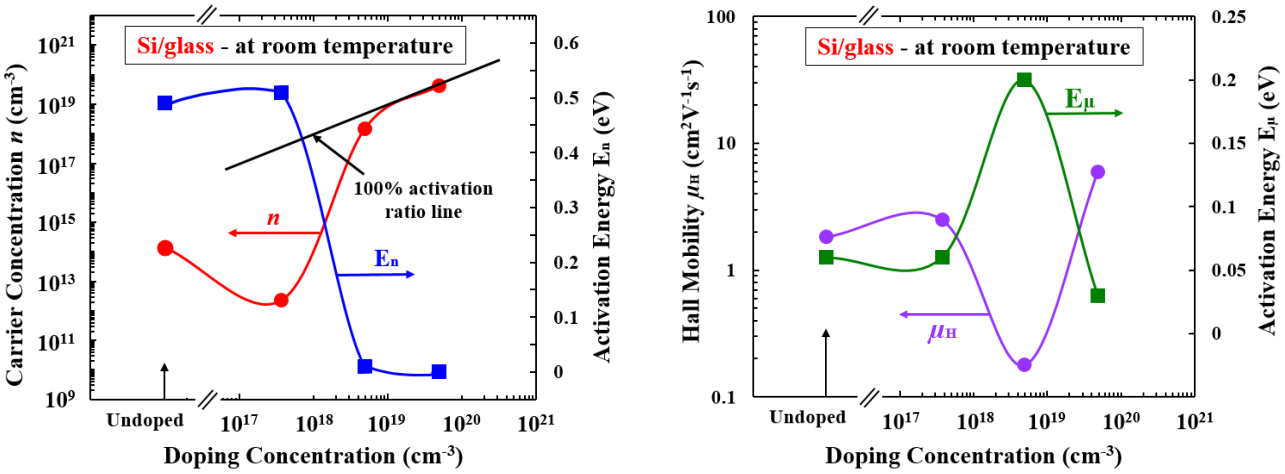

(a) **(b)**

Fig. 9. Mai Thi Kieu Lien and Susumu Horita

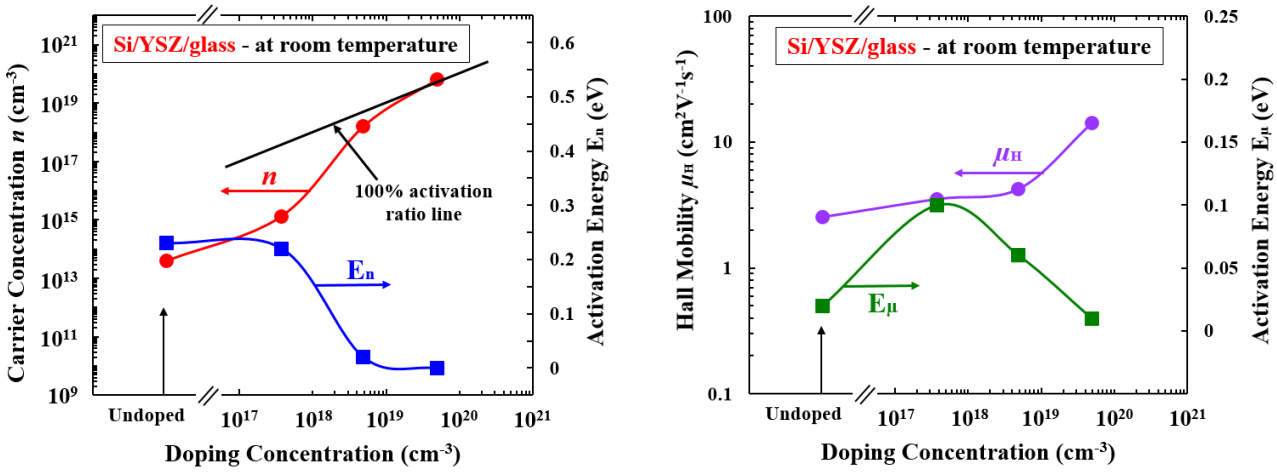

(a) **(b)**

Fig. 10. Mai Thi Kieu Lien and Susumu Horita